Observation of ion acoustic waves associated with plasma-induced incoherence of laser beams using Thomson scattering

H. C. Bandulet, C. Labaune, J. Fuchs, and P. Michel*
Laboratoire pour l'Utilisation des Lasers Intenses (CNRS UMR No. 7605), École Polytechnique–CEA, Université Paris VI, 91128 Palaiseau Cedex, France

J. Myatt
Laboratory for Laser Energetics, University of Rochester, 250 East River Road, Rochester, New York 14623-1299, USA

S. Depierreux
CEA-DIF, Boîte Postale 12, 91680 Bruyères-Le-Châtel, France

H. A. Baldis
Lawrence Livermore National Laboratory and University of California Davis, Livermore, California 94550, USA
(Received 19 March 2003; published 20 November 2003)

We have carried out experiments to investigate the physical processes responsible for the recently discovered phenomenon of plasma-induced incoherence (PII) of a laser beam. Using a Thomson scattering diagnostic, we have observed ion acoustic waves (IAW) having wave vectors transverse to the interaction beam spectral and temporal characteristics of which show a clear correlation with other signatures of PII for various conditions of plasma density and laser intensity. These results support the recent theoretical interpretation for which the IAW result from the coupling between forward stimulated Brillouin scattering and self-focusing of the laser light in PII mechanisms.

DOI: 10.1103/PhysRevE.68.056405 PACS number(s): 52.35.−g, 52.38.−r

I. INTRODUCTION

Over the past few years, experimental [1–5] and theoretical [6–12] studies have demonstrated the ability of an underdense plasma to reduce the spatial and temporal coherence of an intense laser beam propagating through it. As any process affecting laser propagation, plasma-induced incoherence (PII) appears fundamental for inertial confinement fusion (ICF) [13] for it can have an impact on wave-coupling conditions. In fact, the growth rates of convective three-wave instabilities, such as stimulated Brillouin scattering (SBS) or stimulated Raman scattering (SRS) [14] greatly depend upon the beam's level of coherence. The effect of a progressive loss of coherence would be to relax the constraints imposed by the presence of such undesirable parametric instabilities in laser-fusion plasmas. However, while instabilities could be reduced, a lower spatial coherence may spoil the laser's irradiation uniformity through beam spray and hence can be disadvantageous for ICF. A better physical understanding of of PII would aid in assessing the potential benefits for ICF, and may enable control over them.

While most previous experiments have demonstrated the effectiveness of the plasma-induced incoherence of laser beams through measurements of beam characteristics after propagation through the plasma [1–5], none of these have given insight into the underlying mechanisms. Theoretical interpretations [6,10–12,7] explain PII as the result of the interplay between different forward scattering processes such as self-focusing, forward SBS, and the more recent resonant instability of filaments [9]. Simulations performed for our experimental conditions [12] show that the filament instability provides an ion-wave seed for forward SBS of the interaction beam. A broad spectrum of ion acoustic waves (IAW) is thus resonantly excited. These waves have small wave vectors and propagate transversely to the beam. Identification of these waves in an experiment is of outstanding theoretical interest since it would validate part of the proposed scenario.

The experiment presented in this paper was designed to detect the presence of IAW having frequencies and wave numbers according to the numerical simulations of PII [12]. In particular, the simulations demonstrate that transverse IAW fluctuations can be driven at large enough wave numbers to be detected experimentally. A Thomson scattering diagnostic was put into place to look for such IAW and to study their spectral and temporal behavior and their correlation with transmitted light frequency broadening. The spectrum of the transmitted light, a signature of PII, was simultaneously monitored with the Thomson scattered spectra for various interaction conditions. The comparative results give good evidence for the participation of IAW in PII.

II. EXPERIMENTAL SETUP

A. Beam configuration and plasma characteristics

The experiment was performed using six Gaussian 600-ps full width at half maximum (FWHM) laser beams of the Laboratoire pour l'Utilisation des Lasers Intenses facility. All beams were smoothed by random phase plates (RPP) and contained in the horizontal plane. All beams had horizontal

*Also at CEA-DIF, Boîte Postale 12, 91680 Bruyères-Le-Châtel, France.

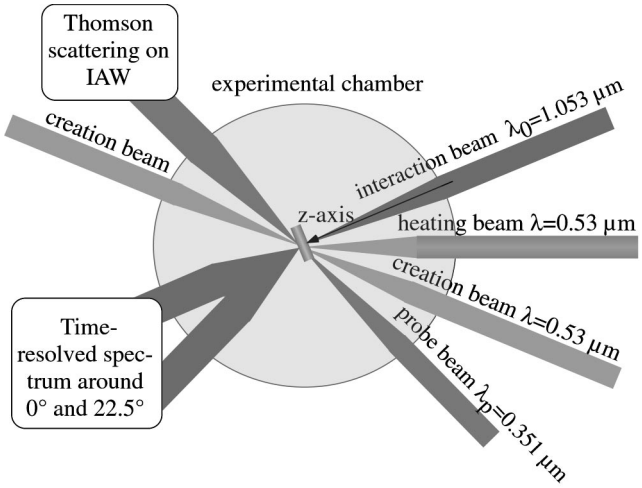

FIG. 1. Layout of the laser beams and main diagnostics. The thin-foil target is at the center of the experimental chamber with its surface perpendicular to the interaction beam.

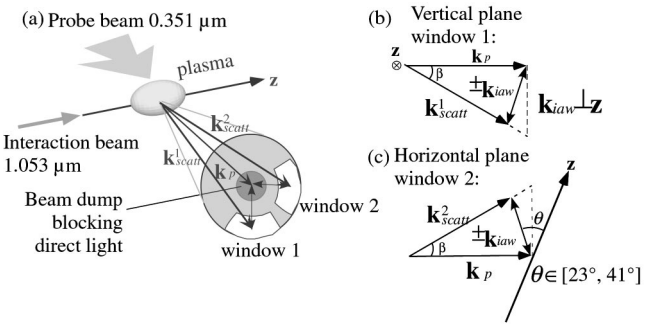

FIG. 2. (a) Thomson scattering of the probe beam ($\mathbf{k}_p$, λ_p) on IAW ($\mathbf{k}_{IAW}$) perpendicular to the interaction beam. Scattered light ($\mathbf{k}_{scatt}$, λ_{scatt}) is collected outside the incident cone over an angular window ranging between 7.7° and 11.3° below the horizontal plane (window 1) and in the horizontal plane (window 2). Wave vector diagram for the Thomson scattering in the vertical window (b) and horizontal window (c). Window 1 collected scattered light with angles θ varying from 73° to 110° and window 2, angles θ varying from 23° to 41° away from the interaction beam.

polarization. The beam configuration is shown in Fig. 1. The plasma was preformed by two counter-propagating laser pulses at $\lambda = 0.53$ μm focused onto the surface of a 1-μm thick parylene (CH) foil target and then heated by a third identical beam 0.6 ns after the first two. The plasma's main expansion axis was perpendicular to the target's initial surface, which we define as the z axis. The target was initially at $z=0$. With a time delay of 1.6 ns after plasma formation, an interaction beam at $\lambda_0 = 1.053$ μm with a maximum average intensity of $\langle I \rangle_{14} = 1$ in units of 10^{14} W/cm^2 and with an initial f/6 aperture was sent propagating along the z axis towards $z>0$. In the following, we will refer to the front part of the plasma as the entrance side of the interaction beam with $z<0$, and the rear part of the plasma as the output side with $z>0$. At the same moment, a low-intensity ($\langle I \rangle_{14} \sim 0.04$, $\lambda_p = 0.351$ μm) probe beam was focused onto the plasma by a f/10 lens at 67.5° from the interaction beam. By reducing the energy of the creation beams from 50 J to 15 J, we obtained two sets of plasma conditions with maximum densities at the peak of the interaction pulse of $0.3n_c$ and $0.8n_c$, respectively, where $n_c = 1 \times 10^{21}$ cm^{-3} is the critical density for 1.053 μm light. The high densities were interesting because they were seen to favor PII in past experiments [4,5]. The plasma's characteristics were similar to those reported in Refs. [4,5,15]. According to two-dimensional(2D) hydrodynamical simulations (see Ref. [15]), the maximum density evolution is best described by an exponential decay in time: $n_{top}(t) = n_{top} \exp[-t/(530 \text{ ps})]$, where $t=0$ corresponds to the peak of the interaction pulse. The typical scale length of the inverse parabolic profile was 700 μm for the low-density plasma and 300 μm for the high-density plasma.

B. Diagnostics

The probe beam was used for Thomson scattering off ion acoustic waves excited by the laser-plasma interaction. The scattered light was collected by a f/2.5 lens and analyzed using a spectrometer-streak camera combination with spectral and temporal resolutions of 0.4 Å and 130 ps, respectively. A beam dump placed on the lens's surface blocked the direct light from being collected [see Fig. 2(a)]. The magnitude and direction of the probed wave vectors were further selected by placing additional masks on the collection optics. Two such apertures were used during the experiment, one in the horizontal plane and one in the vertical plane, as illustrated in Fig. 2. When the properties of the probe beam and the angle of observation have been set, there are two possible ion acoustic waves to satisfy the Thomson geometry: $k_{IAW} = \pm(k_p - k_{scatt})$ [16]. They have opposite directions. The magnitude of the probed wave vector varies with the scattering angle θ_{scatt} according to $k_{IAW} = 2k_0(1 - n_e/n_c)^{1/2} \sin(\theta_{scatt}/2)$, where k_0 is the modulus of the wave vector of the interaction beam in vacuum. For both observation windows, the *scattered* light was collected between $\beta \in [7.7°, 11.3°]$ away from the initial probe axis, which in turn corresponds to ion waves with wave numbers varying from $0.4k_0$ to $0.6k_0$. The direction of the probed IAW is determined by the Thomson scattering geometry. The first aperture (window 1) collected light that scattered off IAW propagating nearly transversely to the interaction beam at angles θ between 73° and 110°. The second aperture (window 2) collected the scattered light off IAW mostly in the horizontal plane with angles θ varying from 23° to 41° away from the interaction beam.

The forward scattered light of the interaction beam was collected within two angular ranges: between $0° \pm 11°$ (up to twice its focusing aperture) and between $22.5° \pm 5.0°$ away from the z axis in the horizontal plane. Light within each aperture was separately analyzed using a spectrometer coupled to a streak camera with spectral and temporal resolutions of (2 Å, 150 ps) for the first aperture and of (2Å, 60 ps) for the second aperture. By placing different masks on the collected light's path we were able to further refine the observation angle within each aperture.

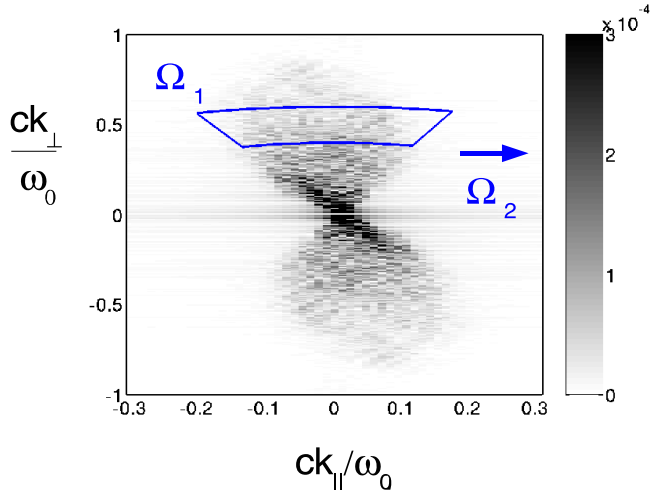

FIG. 3. Magnitude of the two-dimensional spatial finite Fourier transform (FFT) of electron density perturbations, $|\delta n_e/n_0(\vec{k})|$, with normalization such that $\delta n_e/n_0(\vec{x})=\Sigma_{\vec{k}}\delta n_e/n_0(\vec{k})\exp(i\vec{k}\cdot\vec{x})$, where $\vec{k}=(k_{||},k_{\perp})$. The FFT was performed over a $(\Delta z=80\ \mu\text{m})\times(\Delta x_{\perp}=250\ \mu\text{m})$ strip centered at $z=100\ \mu$m, $x_{\perp}=0\ \mu$m, i.e., 100 μm to the rear of the target of the simulation data taken from Ref. [12] that closely reproduce the current experimental conditions. The area marked Ω_1 indicates the wave numbers probed by the Thomson scattering probe with collection window 1 (cf. Fig. 2). The wave numbers probed by the second geometry (window 2) lies slightly outside of the figure in the direction indicated by the arrow labeled Ω_2 with characteristic wave number $\vec{k}=(0.42, 0.26)$.

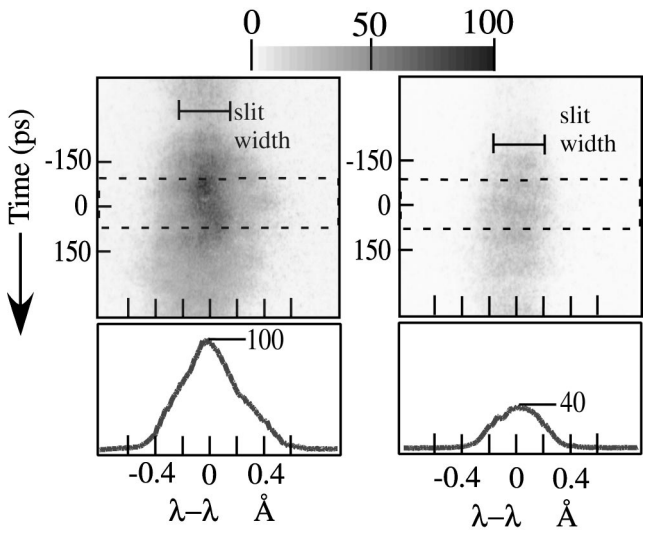

FIG. 4. Time-resolved spectra for the low-density plasma $(n_{top}=0.3n_c)$ of Thomson scattered light at $z=170\ \mu$m in the rear part of the plasma (a) for $\langle I\rangle_{14}\sim 1$ and (b) for $\langle I\rangle_{14}\sim 0.1$. The probe beam is Gaussian with 600 ps FWHM. (c) and (d): spectral intensity profiles integrated over the dashed box.

III. NUMERICAL RESULTS FOR THE DENSITY FLUCTUATION SPECTRUM

The two-dimensional laser-plasma interaction code HARMONHY [12] was used to model our experiment over the whole duration of the interaction pulse ~600 ps with realistic interaction conditions and f/6 RPP optics. The nonlinear hydrodynamic plasma model used by HARMONHY allows us for the use of density and velocity profiles, spatial and temporal dependence of which, due to target expansion, closely mimic those of the experiment as described in detail in Ref. [12]. Furthermore, the paraxial model used for light propagation allows one for the simulation of the whole plasma profile in the z direction. With these features, the simulations correctly describe the interplay between strong inverse Bremsstrahlung absorption, laser pulse temporal profile and target expansion that were found necessary in order to correctly describe the transmitted light spectra.

Simulations with a peak average interaction intensity of $\langle I\rangle_{14}\sim 0.45$ and nonlocal electron heating included along with the ponderomotive force show the generation of a broad spectrum of density fluctuations, evident in Fig. 3, as a result of self-focusing, filament instability, and forward SBS. The frequency spectrum of the transmitted light corresponding to these conditions exhibited a strong redshift ~10 Å that has been attributed to self-phase modulation of laser light brought about by the nonlinear evolution of density channels.

Figure 3 shows the spatial density fluctuation spectrum $|\delta n_e/n_0(\vec{k})|$, taken from the simulations, over a region 100 μm to the rear of the target center where the average density $n_e/n_c=0.25$ at the peak of the interaction pulse. One finds these fluctuations to be contained within angles of $90°\pm 20°$ from the z axis, i.e., nearly transverse to the interaction beam, and extending up to magnitudes of $k_{\perp}\sim 0.7\ \omega_0/c$, where ω_0/c is the vacuum wave number of the interaction beam.

The regions of wave number probed by the Thomson scattering experiment using collection windows 1 and 2 (see Fig. 2) correspond to the areas of $\vec{k}$ space in Fig. 3 that are labeled Ω_1 and Ω_2, respectively. Evaluating $(\delta n/n)_{rms}\equiv\langle(\delta n_e/n_0)^2\rangle^{1/2}$ using Parseval's theorem gives $(\delta n/n)_{rms}=0.009$ for the Thomson scattering volume, where the angle brackets indicate a spatial average. Restricting the sum over wave numbers to include only those wave numbers which are contained within the regions marked Ω_1 and Ω_2 in Fig. 3 gives $[(\delta n/n)_{rms}]_{\vec{k}\in\Omega_1}=3\times 10^{-6}$ and $[(\delta n/n)_{rms}]_{\vec{k}\in\Omega_2}=5\times 10^{-9}$, respectively. On this basis, we would predict that a Thomson scattering diagnostic would see an enhanced signal first experimental geometry (window 1), and a thermal level in the second (window 2). Note that the value of 5×10^{-9} corresponds to the level of numerical noise, and thermal fluctuations are not included in the simulations.

IV. EXPERIMENTAL RESULTS

A. Spectra of Thomson scattered light

Figure 4 shows typical Thomson scattering spectra collected in the vertical window of the diagnostic. The colorbars reflect the relative signal intensity of the Thomson scattered signal and the scale units are consistent between all Thomson spectra. This result has been obtained in the low-density

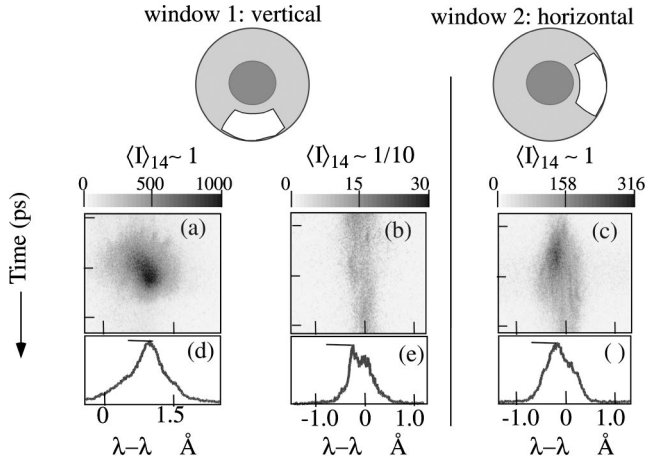

FIG. 5. Comparison of the Thomson scattered spectra between the vertical and horizontal collection window in the high-density plasma ($n_{top}=0.8n_c$). Laser intensities are $\langle I\rangle_{14}\sim 1$, 0.1 in (a), (c), and (b), respectively. The different colorbars provide information on the signals' relative intensities. [(c), (d), and (f)]: time-integrated intensity profiles of the spectra in (a), (b), and (c), respectively.

plasma ($n_{top}\sim 0.3n_c$ and $\langle I\rangle_{14}\sim 1$) for which evidence for PII has already been established in the recent past [4,5]. To demonstrate that these waves were produced by the interaction beam, we reduced its intensity by a factor of ten, $\langle I\rangle_{14}\sim 0.1$, and the corresponding spectrum is shown in Fig. 4(b). For both laser intensities, the diagnostic collected light emitted from a plasma volume of $\Delta z\sim 40$ μm centered at $z=+170$ μm in the rear part of the plasma. By comparison of Figs. 4(a) and 4(b), we observe that the signal obtained at high laser intensity reduces to noise level (due to stray light and/or plasma emission) when the intensity is lowered by a factor of ten. Note that in this case, the limit of sensitivity of the camera has been attained. The strong reduction in signal confirms that the observed signal at $\langle I\rangle_{14}\sim 1$ comes from IAW associated with the interaction beam. The signal peaks at the laser pulse's peak intensity and has an approximate duration of 300 ps. It exhibits a spectral broadening of 0.3 Å on each side of the initial wavelength, with no significant spectral shift. Assuming scattering from density fluctuations associated with forward SBS IAW the expected Thomson scattering spectra would consist of two 0.2-Å wide components symmetrically shifted away from the probe wavelength by about 0.15 Å. The signal's width of 0.2 Å mainly due to the integration over the collection volume of the velocity gradient (Doppler broadening) and the density gradient but also the angular dispersion Δk_{iaw} of the probed ion waves in the collection aperture. Because of the limited spectral resolution of the system, which was at best 0.4 Å only, these two components are likely merged in a broad component as observed in the experimental spectrum.

Since PII is shown to become more effective as the plasma density increases [4,5], we repeated the previous Thomson scattering measurements in a higher density plasma ($n_{top}=0.8$ n_c) for both laser intensities [see Figs. 5(a) and 5(b)]. In this plasma, the scattered light exhibits more complex features and the integrated signal is on the average 40–100 times stronger than in the low-density plasma for the same location on the z axis and same collecting aperture. For $\langle I\rangle_{14}\sim 1$, we observe that the bulk of the signal is now entirely shifted by 1–1.5 Å towards longer wavelengths. Again the signal is greatly diminished, near noise level, when the intensity is divided by a factor of ten. A complementary result comes from the observation of scattered light in the horizontal window which, due to the scattering geometry [Fig. (2)], probes IAW whose wave vectors have a large longitudinal component. The signal [see Fig. 5(c)] associated with nontransverse IAW is dramatically lower than for transverse IAW. Moreover, the signal associated with nontransverse IAW does not exhibit the same nonlinear behavior with increased plasma density or beam intensity. This observation is in agreement with the numerical results discussed in Sec. III.

B. Spectra of the forward scattered interaction beam

Our previous observations of PII were partly based on the spectral analysis of the forward scattered light at $0°\pm 10°$ from the laser axis [4,5]. These spectra displayed a strong redshifted component up to about 10 Å as a result of strong induced temporal incoherence. This red-shift has been correlated with direct measurement of the coherence time using a Michelson interferometer and is considered a clear signature of PII. The IAW wave vectors responsible for the near-forward scattering are of the order of $0.15k_0$. The transverse IAW with $k_{IAW}\in[0.4k_0, 0.6k_0]$ detected by Thomson scattering in this experiment cause the interaction beam to be deflected by angles between 21° and 31° in the vertical plane. Because of mechanical constraints we could only collect the light at such angles in the horizontal plane. The appropriate solution was then to place ourselves in equivalent interaction conditions in the horizontal plane by changing the laser's polarization direction by 90°. We rotated the polarization from horizontal to vertical, using a half-wave plate, and collected the forward scattered light at $22.5°\pm 5.0°$ in the horizontal plane which is associated with the IAW observed by Thomson scattering.

An example of two time-resolved spectra, recorded at 22.5° from the laser axis in the high- and in the low-density plasmas, is shown in Fig. 6. The spectra display a broad redshifted component with a shift larger in the high-density plasma than in the low-density plasma by a factor between two and four. Typical FWHM values of the redshifts for the low- and high-density plasmas are (0–5) Å and (2–16) Å, respectively. These shifts are larger than the ones of the light collected at a smaller angle. The red component is shorter in time than the laser pulse and its maximum intensity coincides with the peak of the interaction pulse. It usually becomes visible little before ($\sim$100 ps) the peak of the interaction pulse in the case of a high plasma density. This is partly due to a rapid increase in transmission, from $\sim$5% at -200 ps to $\sim$35% (i.e., the plasma becomes more transparent), when approaching peak laser intensity. It is noticeable that the observed redshifts are larger than what could be expected from pure forward SBS in the weak coupling regime and that they depend on the laser intensity. Numerical simulations [3,12] have produced a good quantitative agree-

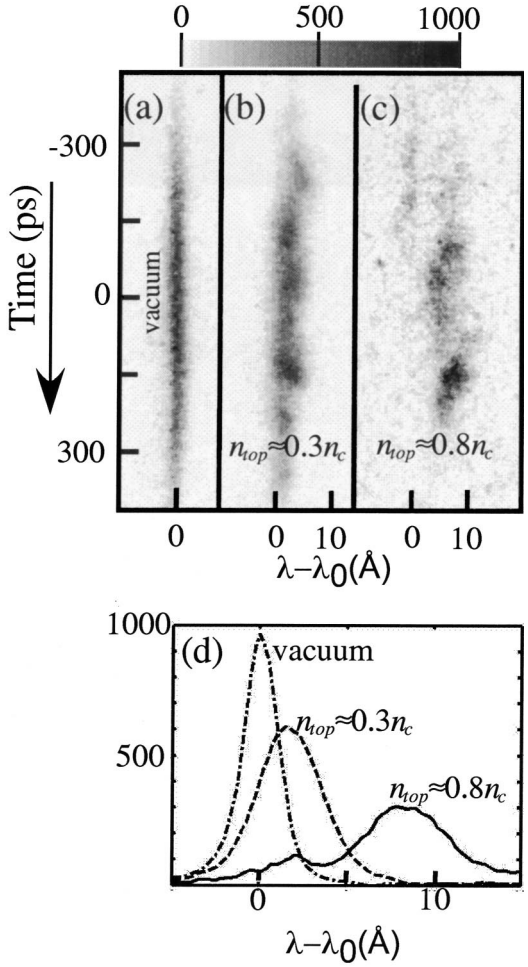

FIG. 6. Transmitted light spectra, collected over angles 22.5° ±5.0°: (a) calibrated in vacuum, (b) in a plasma with $n_{top} \sim 0.3n_c$, and (c) in a plasma with $n_{top} \sim 0.8n_c$. (d) Time-integrated lineouts of the signals in (a), (b), and (c). The spectral resolution is 2 Å. Time 0 corresponds to the peak of the incident beam.

ment of the spectra recorded at 0°±10° based on the self-phase modulation of the forward scattered light in the channels dug by self-focusing with an additional contribution from forward SBS associated with the transverse IAW. This explanation also holds for the light collected at 22.5°.

V. CORRELATION BETWEEN TRANSVERSE IAW AND THE INTERACTION BEAM'S FORWARD SCATTERED LIGHT

We have observed correlations between the observed transverse IAW waves and the transmitted interaction beam at 22.5° in time, intensity, and spectra when the laser intensity or the plasma density was modified.

A. Temporal correlation

The temporal profile of the red component at 22.5° is comparable to that of the Thomson scattered spectra in the high-density plasma since both signals occur near the pulse's peak intensity, and have shorter duration than the laser pulse as shown in Fig. 7. Slight differences in the signal's initial

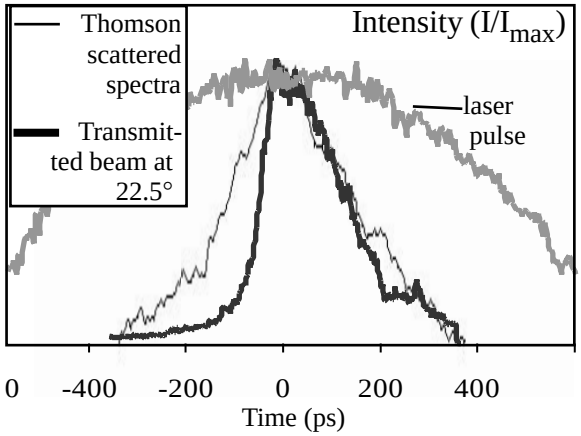

FIG. 7. Temporal evolution of the Thomson scattered signal and that of the redshifted component of the transmitted pulse at 22.5° compared to the initial interaction pulse profile. Each curve is drawn in normalized units of signal intensity.

growth can be explained by a combination of different reasons. As mentioned before, the plasma is very opaque to the interaction beam in the first half of the its pulse. Since the nonlinear phenomena responsible for the existence of the redshift also become more efficient as the peak approaches, the redshifted signal can rapidly rise. The frequency-tripled probe beam, on the other hand, can propagate with little absorption, as the plasma is transparent for 0.351 μm light. The dissimilarity can be worsened by the lack of temporal resolution of the Thomson spectra and to some extent by the fact that the spectrum of transmitted interaction beam is integrated over the whole plasma length (all z's) while the Thomson spectra is collected over a small region on the z axis and so can only account for the growth of local IAW.

B. Intensity correlation

Comparison of the redshifted component in the transmitted light spectra at 22.5° with the ion acoustic wave signal also show a good correlation between the two phenomena as a function of the laser intensity. Like the IAW signal, the red component of the transmitted light decreased strongly when the laser intensity was reduced by a factor of ten, demonstrating the nonlinear behavior of the involved processes.

A further correlation between both types of spectra was made by flipping the beam polarization from the horizontal to the vertical plane. Note that for each diagnostic the signals were recorded under the same observation conditions for both polarization states. The Thomson scattered light was collected in window 1 and the forward scattered light of the interaction beam was selected in the vertical plane only. This way, both the interaction beam and the probe beam scattered off vertical IAW. For this purpose, and because of the mechanical constraints stated earlier, the effect of the beam's polarization state on the transmitted interaction beam was tested for near-forward transmission (i.e., between 8° ±3°). Figure 8 shows time-integrated lineouts of the spectra of light scattered by angles between 5° and 11° away from the z axis and the corresponding Thomson scattering spectra for both polarization states of the interaction beam. The sig-

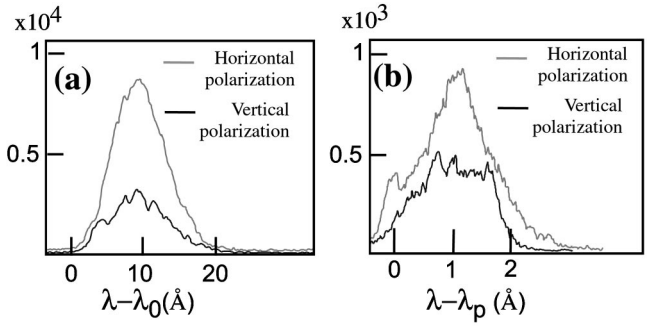

FIG. 8. Time-integrated (over 150 ps) spectral lineouts of the transmitted light (a) and of the Thomson-scattered probe beam off IAW (b) for horizontal and vertical polarization in a high-density plasma ($n_{top}=0.8n_c$ and $\langle I\rangle_{14}\sim 1$). λ_p is the probe wavelength and λ_0 the wavelength of the interaction beam. The forward scattered light is collected in the vertical plane only at $8°\pm 3°$. Intensity values are given in the units of relative measured intensity.

nals have been integrated over 150 ps around maximum signal. A very clear simultaneous reduction of both signals was observed by changing from the horizontal to the vertical polarization. The integrated intensity of the transmitted light's red component drops to $\sim 35\%$ in the vertical polarization state. For this particular location on the z axis, the integrated signal of the Thomson scattering spectra is half than that of the total signal in the horizontal state. Instrumental response was tested to be independent of the light's polarization state and therefore cannot account for any of the changes. In addition to the correlated modification of the two signals, these results show that the light scattering, as well as the generation of the driven IAW, seems to occur preferentially out of the plane of polarization of the laser.

C. Spectral correlation

Both the scattered light of the interaction beam at 22.5° and the Thomson scattered spectra display a strong redshift in the high-density plasma. In these conditions, the plasma response is expected to be both nonlinear and nonlocal, a case for which no complete model exists. Nevertheless, the strong redshift of the Thomson scattered light in the high-density plasma could be produced by a combination of three mechanisms: the Doppler shift, strongly coupled SBS, and/or self-phase modulation of the scattered light off IAW localized in the density channels dug by the interaction beam, whose density varies rapidly. First, the wave vector probed in the plasma by Thomson scattering using window 1 is almost orthogonal to the plasma expansion axis. Unless there is a significant radial flow, the projection of the flow velocity on the probed wave vector would be too small to give the required redshift. Besides, if radial expansion were important, the Doppler shift would be appreciable in the low-density plasma case as well, which it is not. Forward SBS becomes strongly coupled at an intensity of approximately $I=5\times 10^{13}$ W/cm^2 when its mean growth rate exceeds the ion-wave frequency ($\gamma \geqslant \omega_{IAW}$) [6,17]. The fraction of laser speckles that meet the above condition could produce strongly coupled SBS and hence shift the light further towards the red. Shifts up to several times the ion acoustic frequency have been detected by Young [17] in the case of SBS backscattering of the main beam. This additional redshift is, however, still very difficult to predict quantitatively. Regarding the third explanation, the shift in wavelength due to self-phase modulation $\delta\lambda_p$ will be smaller for the probe beam compared to the interaction beam because of its shorter wavelength and shorter length of propagation in the speckles and in the overall plasma. Simple estimates based on the analytical formula [9], $\delta\lambda_p=(N\lambda_p\delta z/2c)[1-n_e/n_c(\lambda_p)]^{-1/2}\{\mathrm{d}[n_e/n_c(\lambda_p)]/\mathrm{d}t\}$ show that a shift of 2Å could be obtained with realistic values of the density decrease as a function of time ($dn\sim 0.1n_c$ in $dt=60$ ps), of the propagation length in each channel ($\delta z\sim 10$ μm), and of the number of channels encountered ($N=10$). In the low-density plasma, this shift would be much smaller, in agreement with Figs. 4(b) and 6(b) showing reduced shifts in the low-density plasma. In this scenario, self-phase modulation would therefore be responsible for the redshift of both the transmitted light and the Thomson scattered light off the transverse IAW associated with the temporal incoherence of the interaction beam.

VI. CONCLUSION

In conclusion, we have observed ion acoustic waves propagating transversely to the interaction beams which are strongly correlated with PII signatures, namely, the frequency broadening of the interaction beam. The observed correlation persisted as density, laser intensity, and polarization states were modified. The presence of a strong Thomson scattering signal in the geometry of window 1 only is consistent with predictions of numerical simulations. In addition, the spectral characteristics of these ion waves are also in agreement with numerical simulations in the case of low plasma density. For the high plasma density the Thomson scatter spectra show a red feature that is shifted by almost 1.5 Å. We have discussed the possible origins for this shift, and have shown that phase modulation by plasma channels associated with the interaction beam is a likely explanation. The observations reported here provide strong experimental evidence for the participation of transverse ion acoustic waves in the PII mechanism. They are important as they will provide a unique access to the study of the influence of PII on parametric instabilities, namely, of ion acoustic waves and electron plasma waves associated with SBS and SRS, respectively.

ACKNOWLEDGMENTS

The authors gratefully acknowledge very valuable discussions with D. Pesme and V. Tikhonchuk who inspired this work. One of the authors (J.M.) would also like to acknowledge discussions with Andrei Maximov. The support of A. Michard and of the technical groups of LULI are also acknowledged. Part of this work was performed under the auspices of the U.S. Department of Energy by University of California Lawrence Livermore National Laboratory under Contract No. W-7405-ENG-48.

[1] P. Young *et al.*, Phys. Plasmas **2**, 2825 (1995).
[2] J. Moody *et al.*, Phys. Rev. Lett. **83**, 1783 (1999).
[3] C. Labaune *et al.*, C. R. Acad. Sci., Ser IV: Phys. Astrophys. **1**(6), 727 (2000).
[4] J. Fuchs *et al.*, Phys. Rev. Lett. **86**, 432 (2001).
[5] J. Fuchs *et al.*, Phys. Rev. Lett. **88**, 195003 (2002).
[6] V.V. Eliseev *et al.*, Phys. Plasmas **4**, 4333 (1997).
[7] A. Schmitt and B. Afeyan, Phys. Plasmas **5**, 503 (1998).
[8] C. Still *et al.*, Phys. Plasmas **53**, 1057 (2000).
[9] D. Pesme *et al.*, Phys. Rev. Lett. **84**, 278 (2000).
[10] G. Riazuelo and G. Bonnaud, Phys. Plasmas **7**, 3841 (2000).
[11] A. Maximov *et al.*, Phys. Plasmas **8**, 1319 (2001).
[12] J. Myatt *et al.*, Phys. Rev. Lett. **87**, 255003 (2001).
[13] J. Lindl, Phys. Plasmas **2**, 3933 (1995).
[14] W. Kruer, *The Physics of Laser-Plasma Interactions* (Addison-Wesley, New York, 1988).
[15] J. Fuchs *et al.*, Phys. Plasmas **7**, 4659 (2000).
[16] J. Sheffield, *Plasma Scattering of Electromagnetic Radiation* (Academic, London, 1975).
[17] P. Young *et al.*, Phys. Rev. Lett. **73**, 2051 (1994).